UCRL-JC-130028
PREPRINT

Application of Adaptive Optics for Controlling the NIF Laser Performance and Spot Size

R. Sacks, J. Auerbach, E. Bliss,
M. Henesian, J. Lawson, K. Manes,
P. Renard, T. Salmon, J. Trenholme,
W. Williams, S. Winters, and R. Zacharias

This paper was prepared for submittal to the
Third Annual International Conference on
Solid State Lasers for Application (SSLA)
to Inertial Confinement Fusion (ICF)
Monterey, California
June 7-12, 1998

August 17, 1998

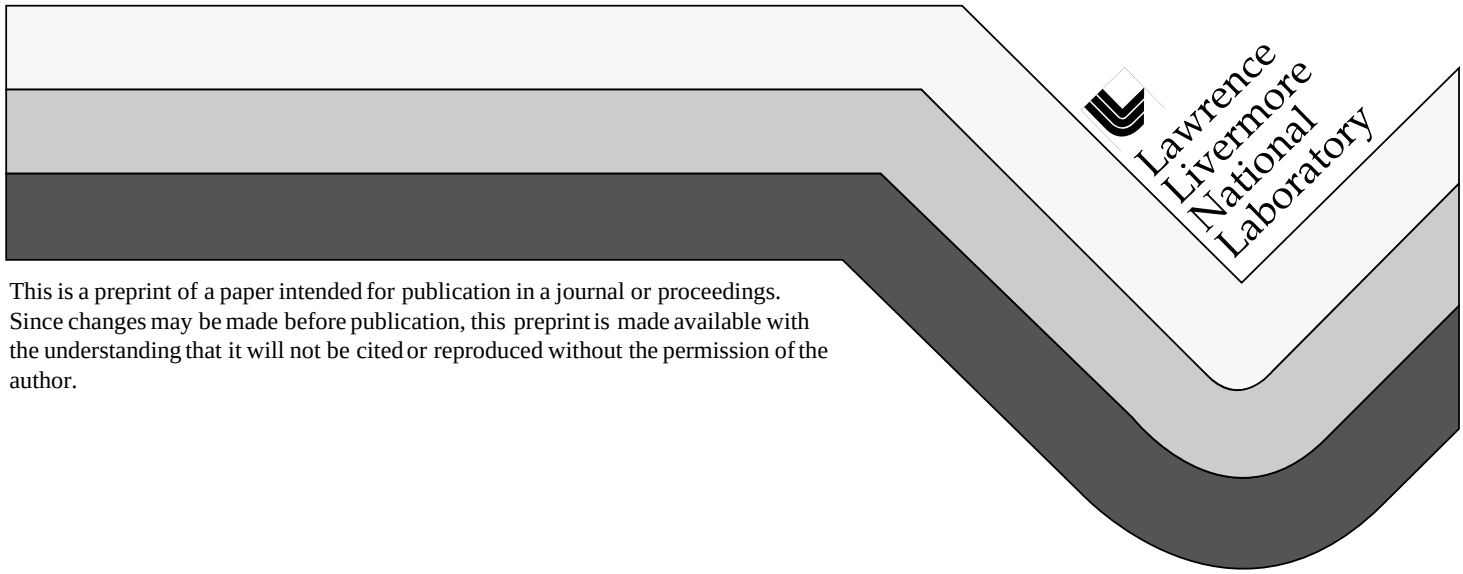

UCRL-JC-130028

Application of adaptive optics for controlling the NIF laser performance and spot size

R. Sacks, J. Auerbach, E. Bliss, M. Henesian, J. Lawson, K. Manes, P. Renard, T. Salmon, J. Trenholme, W. Williams, S. Winters, and R. Zacharias

Lawrence Livermore National Laboratory
Livermore, California 94550

Abstract

The National Ignition Facility (NIF) laser will use a 192-beam multi-pass architecture capable of delivering several MJ of UV energy in temporal pulse formats varying from sub-ns square to 20 ns precisely-defined high-contrast shapes. Each beam wavefront will be subjected to effects of optics inhomogeneities, figuring errors, mounting distortions, prompt and slow thermal effects from flashlamps, driven and passive air-path turbulence, and gravity-driven deformations. A 39-actuator intra-cavity deformable mirror, controlled by data from a 77-lenslet Hartman sensor will be used to correct these wavefront aberrations and thus to assure that stringent farfield spot requirements are met.

We have developed numerical models for the expected distortions, the operation of the adaptive optic system, and the anticipated effects on beam propagation, component damage, frequency conversion, and target-plane energy distribution. These models have been extensively validated against data from LLNL's Beamlet, and Amplab lasers. We review the expected beam wavefront aberrations and their potential for adverse effects on the laser performance, describe our model of the corrective system operation, and display our predictions for corrected-beam operation of the NIF laser.

1. Aberration Sources

The NIF optical chain begins with a single fiber oscillator and ends with 192 separate beams each carrying about 10 kJ of UV energy converging on the target chamber center. In between, there are fiber amplifiers and beam splitters, modulators to add bandwidth, a regenerative ring amplifier, a four-pass rod preamplifier module (PAM), a preamplifier beam transport system (PABTS) including a four-way split, a compound injection telescope, an 11-slab four-pass amplifier cavity, a two-pass five-slab power amplifier, four or five transport mirrors (depending on beam line), and a final optics assembly (FOA) consisting of a vacuum window, two frequency conversion crystals, a final-focus lens, two diffractive optics, and a debris shield. Figure 1 shows an optical layout of the laser, from PAM input to target, illustrating the large number of optics present. Each of these optics will contribute wavefront

errors—from figuring errors, mounting and gravitational stresses, rotational alignment of lenses, and thermal effects. Additionally, since the entire beam path up to the FOA is filled with either air or argon, there will be aberrations due to gas turbulence and acompanying density variations that vary with time scales ranging from milliseconds to seconds.

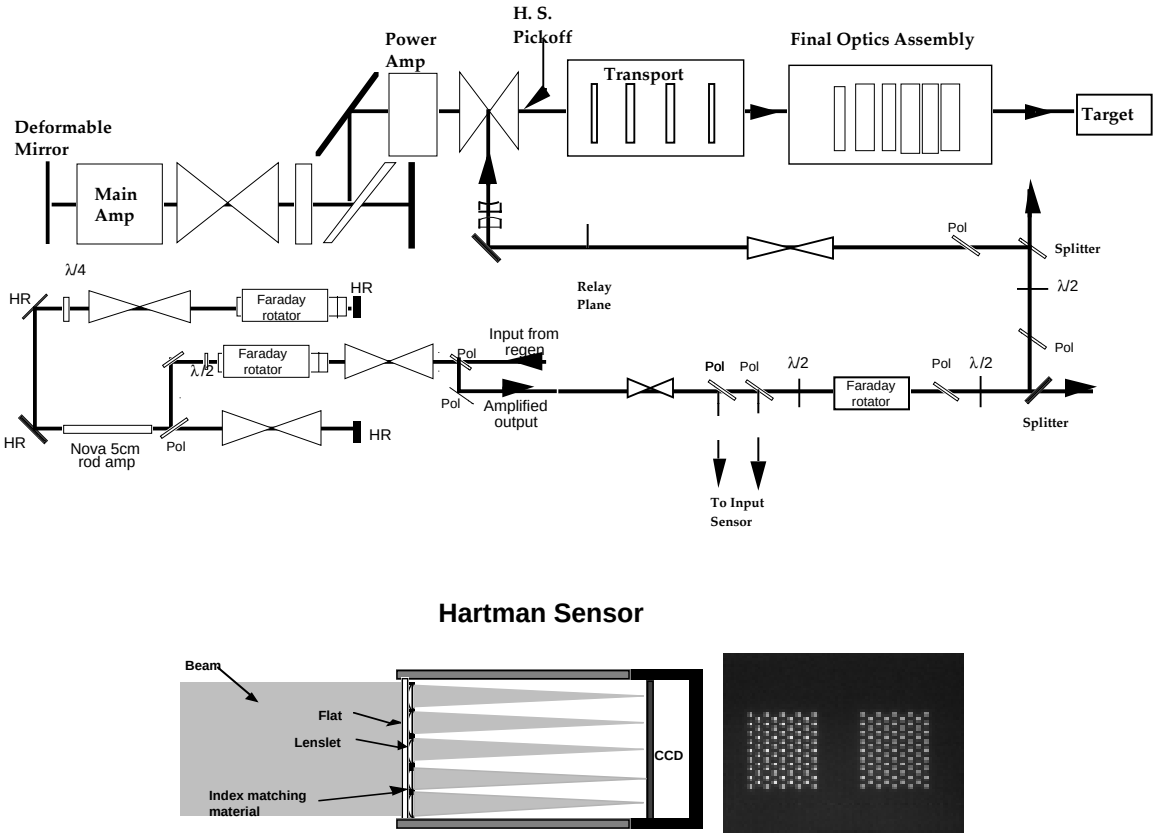

Figure 1. NIF optical chain layout from PAM input to target, showing DM location in the main amplifier cavity and beam sampler location for Hartman wavefront sensor.

We have constructed a Prop92 propagation model describing the optical path shown in Fig. (1). Numerical aberration files, based on measurements of representative parts and projection to NIF production quality[(1)], are associated with each optic and with the overall gas-path influence. Figures (2) and (3) show the phase modification and its power spectral density for a few selected components. As can be seen, amplifier slab aberrations are dominated by the very large, long-scale-length prompt thermal distortions, while the Faraday rotators in the PAM and PABTS display imperfections over a broad range of scale lengths.

The NIF facility is required to be able to deliver 1.8 MJ—9.375kJ per beam—with specified temporal shape inside a 600 μm diameter spot at the target focal plane. Calculating the propagation of an appropriately-shaped beam through our baseline model predicts that without wavefront correction a typical beam at the entrance to the target chamber will have the nearfield

and farfield characteristics shown in Fig. (4). The large ring-up along the positive-x edge is caused by clipping at a spatial-filter pinhole, and results in nearfield fluence some 1.7× the expected damage threshold. The focal-plane radius inside of which 80% of the energy falls is 52 μr (800 μm diameter), and the energy inside 600 μm diameter is 6.875 kJ (1.32 MJ for 192 beams). Clearly, wavefront correction is needed to meet the NIF system design requirement.

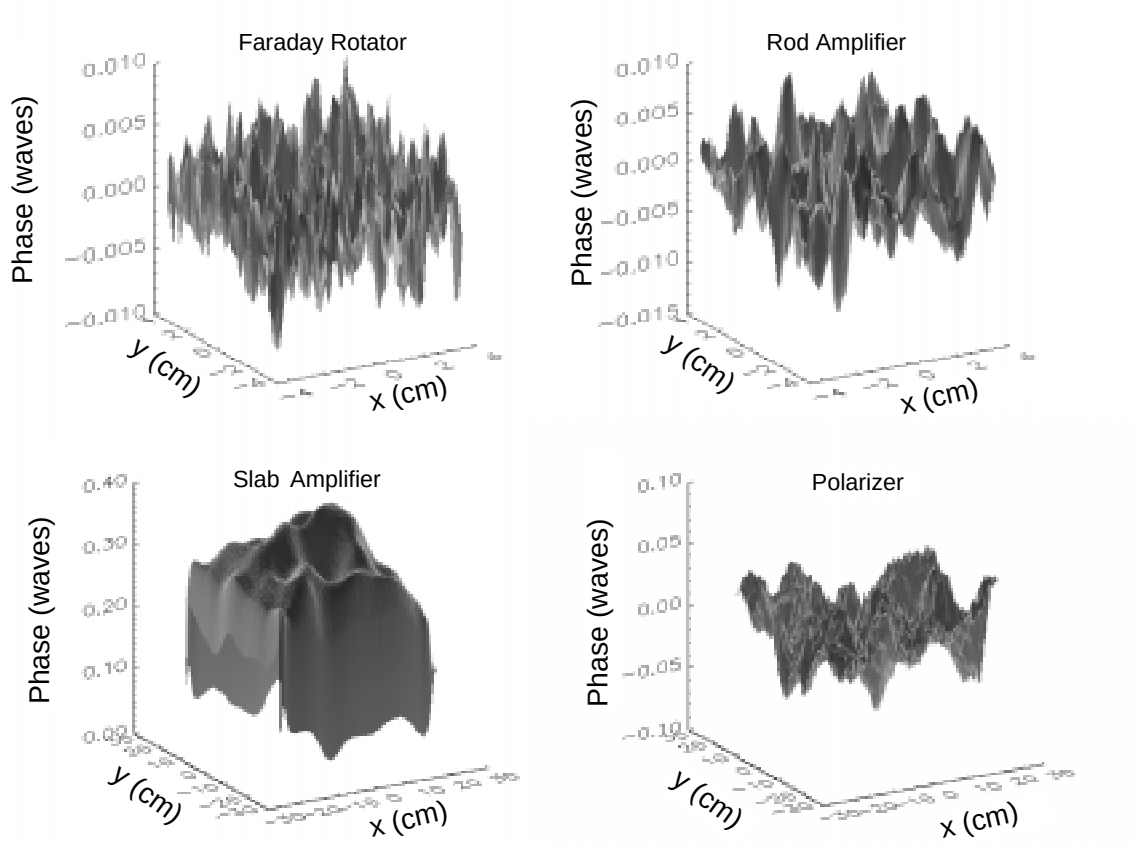

Figure 2. Phase screens depicting optical aberrations caused by four representative elements in the NIF optical chain.

2. Wavefront Correction Model

As shown in Fig. (1), the NIF baseline design calls for wavefront control to be implemented by deploying a 39-actuator square deformable mirror (DM) on the amplifier side of the full-aperture cavity. Since the beam reflects from this mirror twice, physical stroke on the mirror surface yields a 4× effect on wavefront. The wavefront is sensed by a 77-lenslet Hartman sensor located in the output sensor and viewing a cw diagnostic beam sampled by a beam splitter located just past the output lens of the transport spatial filter (SF4)—also shown in Fig. (1).

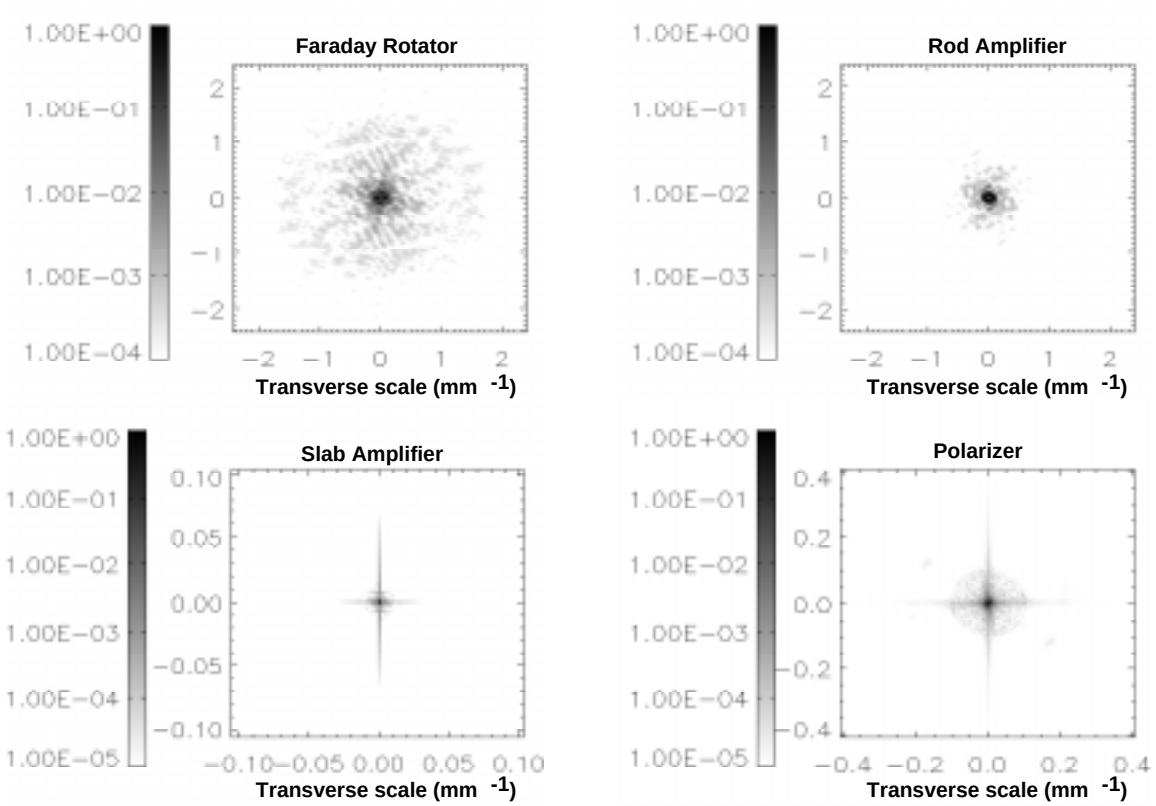

Figure 3. Power spectral density of the phase screens shown in Fig. (2), all normalized to a maximum value of 1. Note the changes in axis scales. The amplifier slabs are dominated by long-scale thermal effects; the figuring errors resemble those shown for the large-aperture polarizer. The small-apertre optics naturally have more short-scale structure.

The wavefront control loop is displayed in Fig. (5). A wavefront reference source—a single mode fiber defining a point source at the pass-4 pinhole plane of the transport filter—is sensed and defines the flat-beam spot centroid locations. Spot centroids from the diagnostic beam are next sampled, and their displacements from the reference source locations measure the local tilts of the wavefront. The actuator influence matrix, calibrated offline, translates the spot displacements into required actuator movements which are communicated to the DM by the mirror control algorithm. This process is iterated closed-loop with a 1 Hz response, both to allow iterative improvement of the correction and to account for time-varying effects such as gas-path turbulence. A few minutes before the shot, a set of pre-determined spot displacements is added to to set-point locations to pre-correct for prompt thermal distortions. One second before shot time, the loop is opened, freezing the correction. The shot wavefront is then measured and used to update the thermal-distortion spot offsets.

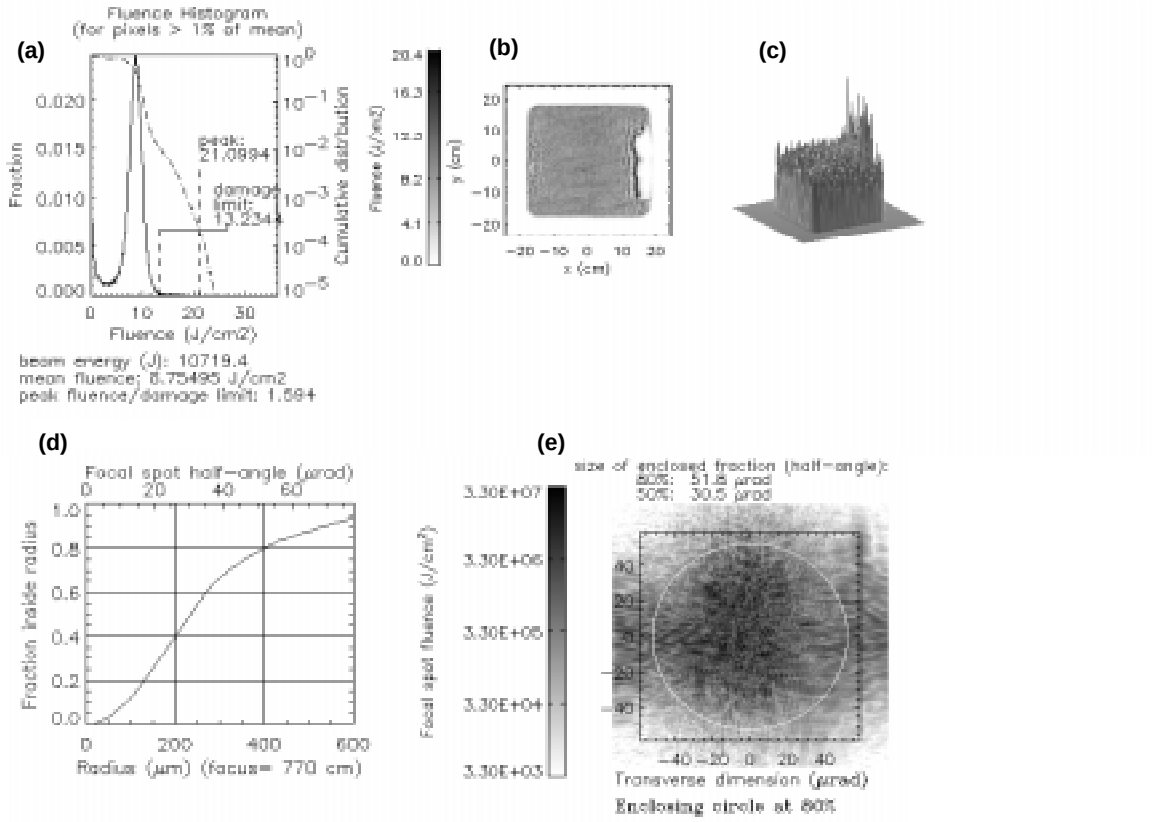

Figure 4. Baseline NIF performance *in the absence of wavefront correction*. (a), (b), and (c) describe nearfield at the tripler exit face. (a) presents a histogram (solid curve) and cumulative distribution (broken curve) of the near-field fluence. "Fraction" means the number of pixels lying in the fluence bucket divided by the number of pixels whose fluence is greater than 1% of the maximum. The cumulative distribution presents the fraction of pixels above the corresponding fluence. (b) and (c) present the spatial distribution of the nearfield fluence. (d) and (e) describe the spatial distribution of energy arriving at the target plane: (e) shows the 2D distribution, and (d) gives the total energy lying inside circles of varying radius.

Prop92 includes the ability to dump a copy of the complex array describing the laser field at any point in the calculation. We have used this feature to develop a post-processor-based model of the adaptive optic (AO) system described above. This model is described in Fig. (6). We first calculate the evolution of a low-power, temporally-flat beam during propagation through the laser chain out to the diagnostic beam splitter—representing the cw diagnostic beam. The dump file describing this beam is read by the post-processor, and a single vacuum propagation step to a relay plane of the DM models the Hartman sensor relay optics. Seventy seven distinct circular subapertures are individually taken to the farfield, and the location of the centroid of each spot is calculated as

$$\bar{x} = \sum_j x_j I_j$$
$$\bar{y} = \sum_j y_j I_j \qquad (1)$$

where the sums are over all gridpoints within the given sub-aperture, the coordinates x_j and y_j are positions in the lenslet focal plane, and $\hat{I}_j$ is the farfield intensity at the j'th pixel. By expressing the centroid displacements as angles, we identify them as the wavefront tilt averaged over the subaperture.

The actuator influence matrix is calculated by a procedure that exactly mimics the method used in the AO controller. Each actuator, in turn, is "moved" by a unit displacement, the resulting influence function (DM surface shape) is imposed as the phase of an otherwise-smooth beam, and the displacement of all 77 spot centroids is calculated. The 39×154 singular value decomposition of this matrix is then the matrix which, when multiplied by a given vector of centroid displacements yields a vector of actuator throws that will minimize (in a least-squares sense) the resulting corrected displacements. This set of actuator throws, and the known influence functions for each of the actuators, yields the desired mirror shape. Since the model aberrations do not change, there is no need to mock up the closed loop aspect of the control system.

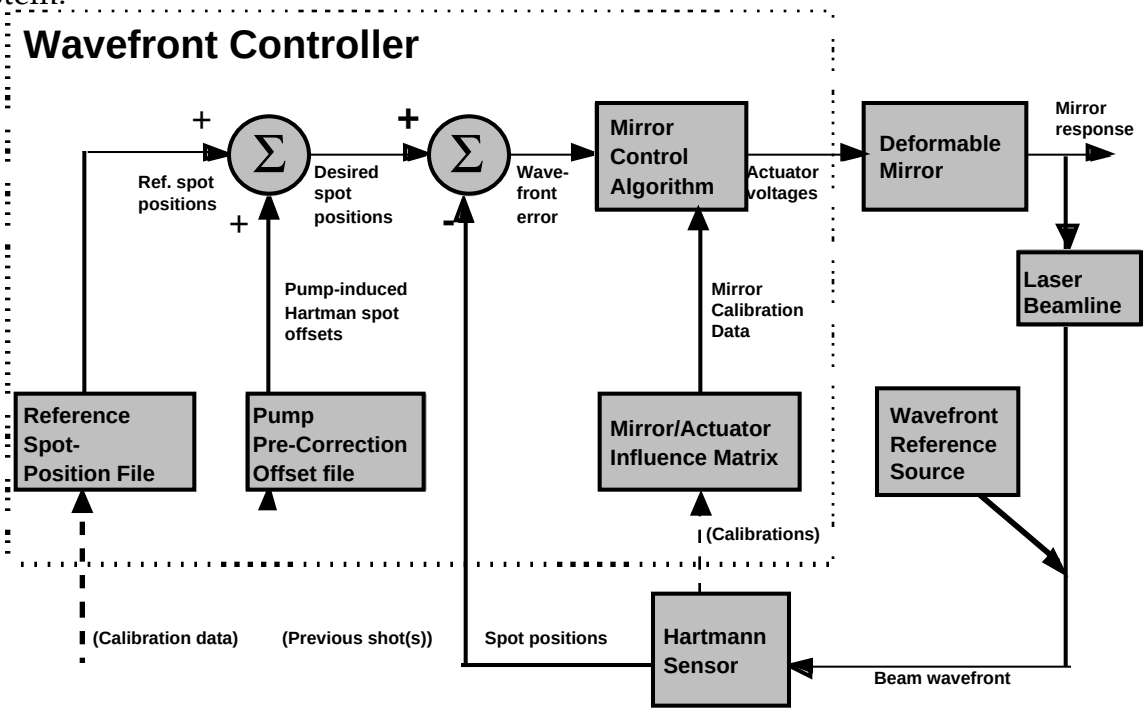

Figure 5. NIF wavefront control loop. Static and slowly-varying aberrations are corrected in closed-loop based on Hartman-sensor measurements, a pre-calculated influence matrix, and pre-determined spot offsets for prompt thermal distortions.

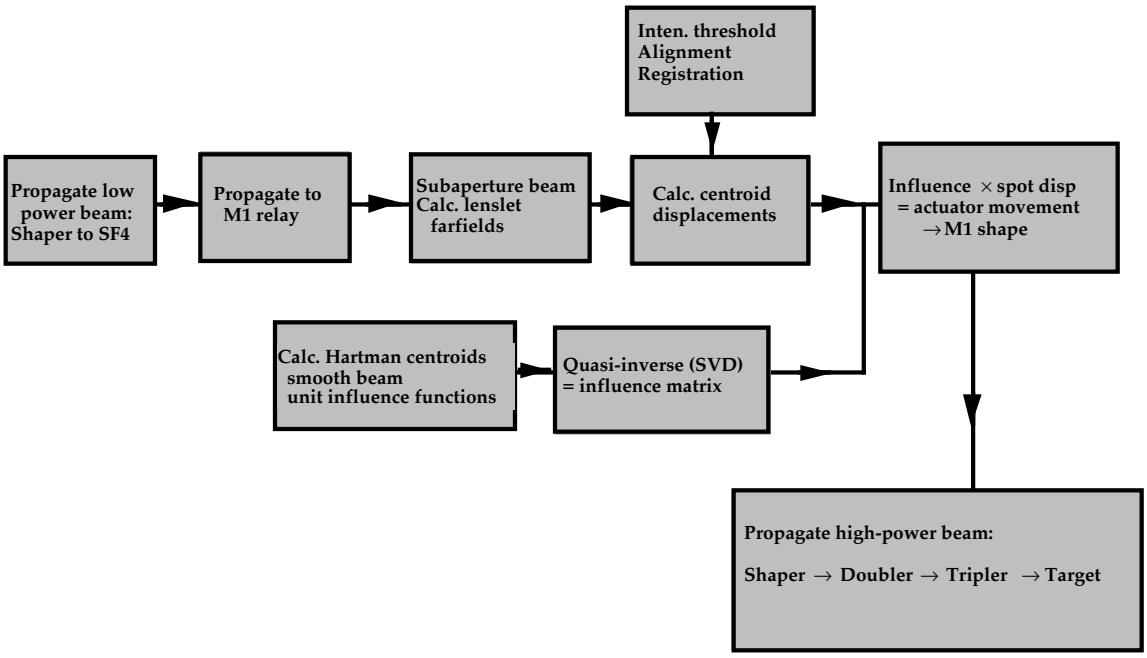

Figure 6. A numerical model captures the salient features of the adaptive optic system.

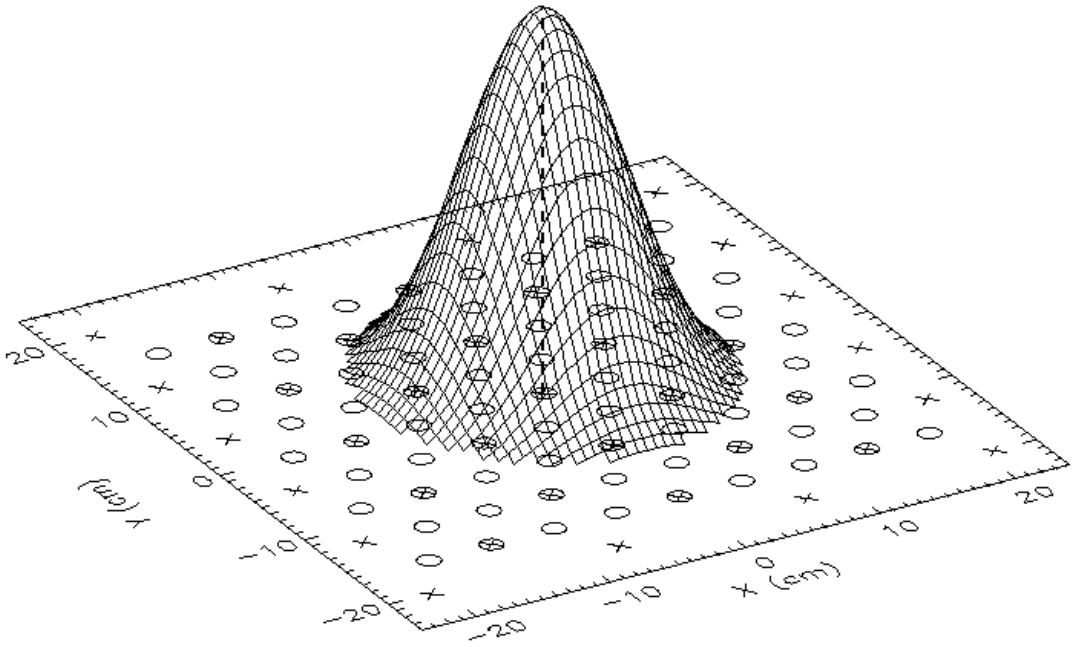

Figure 7. Deformable mirror and Hartman sensor geometry. Since the Hartman sensor is located at a relay plane of the DM, the two may be visualized as if they coincided. Shown here, at the equivalent full-aperture size, are the actuator locations (X's), lenslet locations (O's), and the central-actuator influence function (cut off at 5% of maximum).

The results reported here utilize a single Gaussian influence function shape for all actuators. Although finite-element modeling indicates that this is an excellent approximation for interior actuators, we are actively working to obtain and incorporate more accurate position-dependent influence functions—both through measurement of characteristic devices and through detailed finite element analysis. Figure (7) shows the location of the images of the actuator locations (X's), the Hartman lenslets (circles) and the overlap of the central actuator influence function. The assumption here is that when one actuator is displaced, its neighbors are not held fixed but rather move in concert against a linear restoring force. Relative stiffnesses are chosen so that the influence function decreases by approximately 1/e at the nearest-neighbor location.

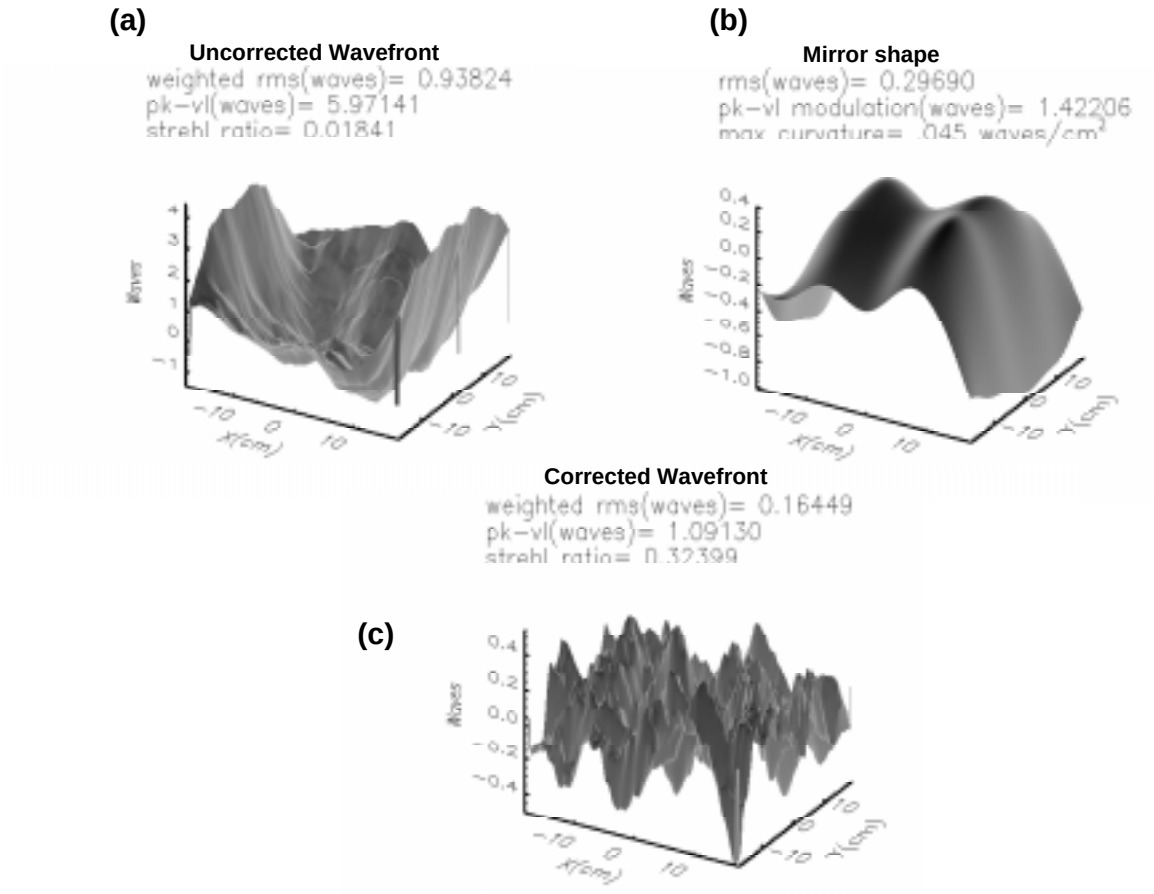

Figure 8. Wavefront correction of the NIF baseline design. The aberrated wavefront of the uncorrected beam (a) is well-corrected by an achievable DM shape (b) generated by our algorithm. The remaining residual wavefront (c) exhibits a six-fold decrease in amplitude and an 18× increase in strehl ratio.

3. Performance

Figure (8) illustrates the degree to which we predict that the NIF wavefront can be cleaned up by the action of the baseline AO system. Shown are the wavefront of the uncorrected low-power beam, the mirror shape generated as a sum of Gaussian influence functions, and the residual wavefront generated by adding the two (with an additional factor of four on the correction to account for the two reflections). As is seen, virtually all long-wavelength structure has been removed, resulting in a decrease by about 6× in both the rms and the peak-to-valley of the beam phase, and a corresponding large increase in beam strehl ratio.

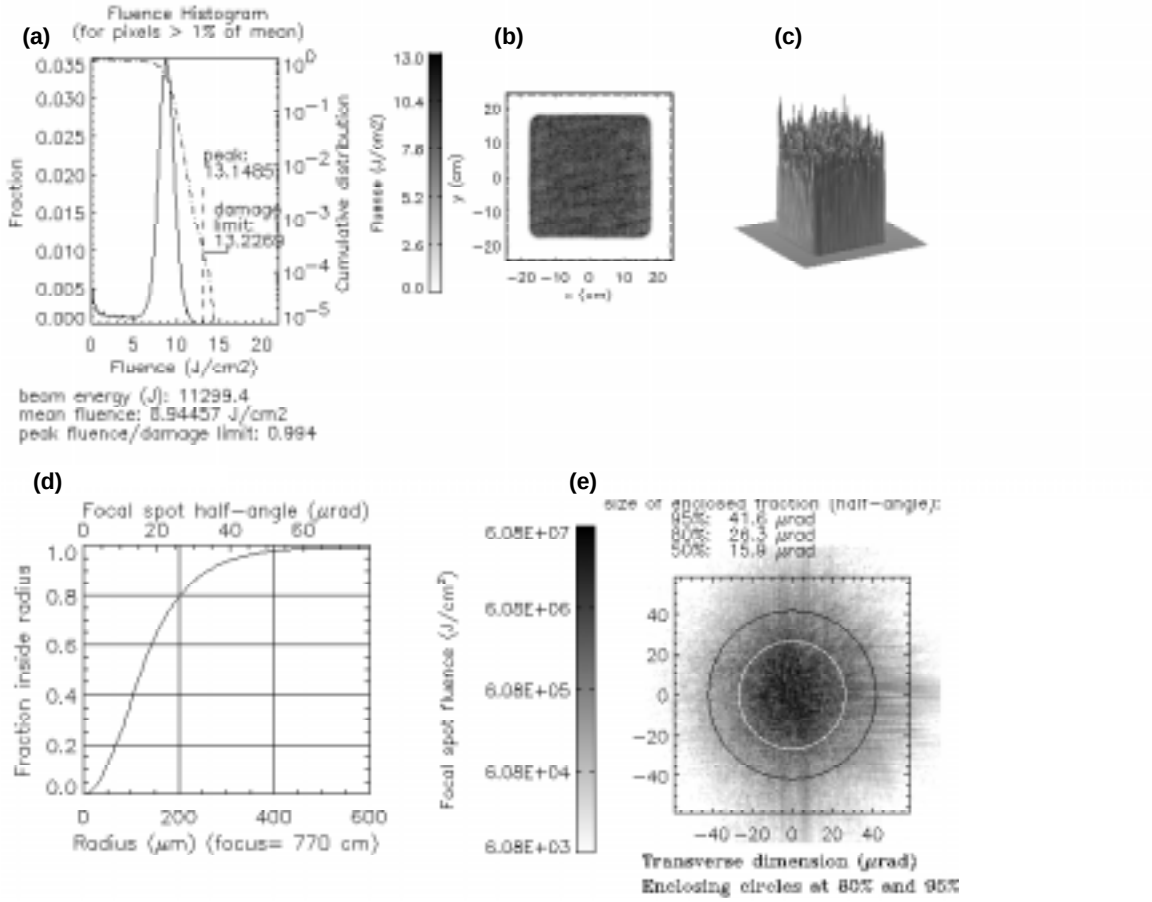

Figure 9. Baseline NIF performance with wavefront correction. Information is presented in the same format as in Fig. (4). Wavefront correction has removed the high-intensity ripples in the nearfield, allowing more energy to be delivered without exceeding the damage limit. In the target plane, 80% of the energy now falls inside a 400 μm diameter circle. The energy inside 600 μm is 10.0 kJ—1.92 MJ for 192 beams.

The effect of this wavefront correction is shown in Fig. (9). The nearfield modulation at the beam edge is nearly eliminated and the farfield 80% spot radius is decreased by nearly a factor of 2. Our prediction is that with this correction we will be able to deliver 1.92 MJ of 3ω energy into the required 600 μm diameter spot while holding the peak fluence below the damage limit on any of the chain optics.

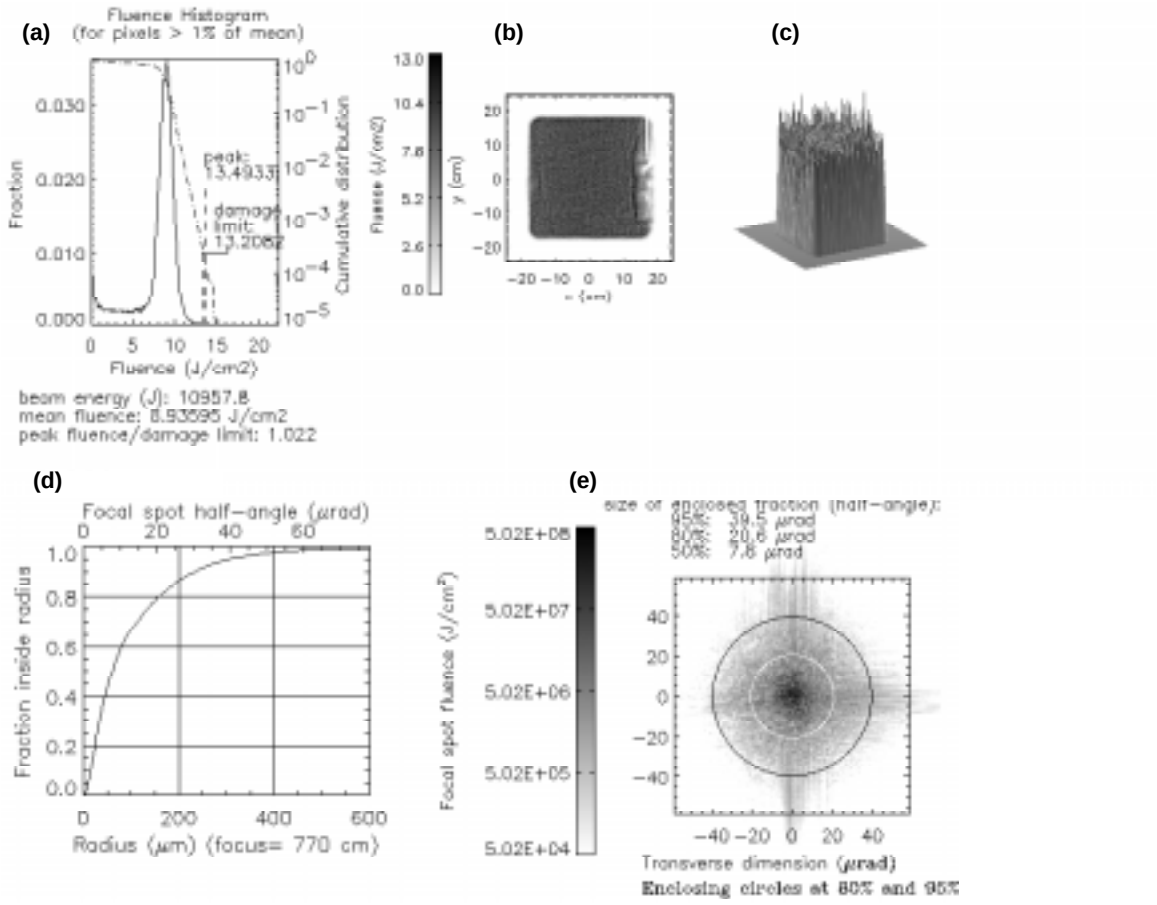

Figure 10. Baseline NIF performance with the addition of a static phase corrector in the PABTS. The farfield spot is substantially sharpened by removal of phase features at shorter scale length.

In Fig. (10), we briefly touch on an advanced concept more fully developed in an accompanying paper[(2)]. Two disadvantages to relying on a DM for wavefront control are its limited spatial spectral response and its limited range of actuator motion. Both of these drawbacks can apparently be substantially alleviated by inclusion in the optical chain of a static corrector, individually matched to each beamline, constructed to remove the static component of the aberrations. In Fig. (10), we place our static corrector in the front end—at the point marked "relay plane" in Fig. (1), which relays onto the DM location. The phase screen is constructed by Fourier filtering the phase of a low power beam sampled at the end of the 1ω chain, retaining structure

longer than 100 μm. Figure (10) compares the resulting high-power nearfield and farfield to those of the baseline calculation, showing that if more design margin is needed, this approach could substantially improve the system performance.

4. Conclusion

A comprehensive Prop92-based simulation of the NIF baseline design, including adaptive optic wavefront correction, has been constructed. The model includes descriptions of the expected aberrations associated with each of the optics in the chain as well as a faithful representation of the AO control system. These aberrations are sufficiently severe that NIF must include wavefront correction in order to fulfill its functional design requirements. We predict that with the baseline correction system NIF will meet its required nearfield and farfield beam characteristics and that the inclusion of non-baseline improvements such as a static corrector could add substantially to the design margin.

*Work performed under the auspices of the U.S. Department of Energy by Lawrence Livermore National Laboratory under Contract No. W-7405-Eng-48.

References

1. J. Lawson, D. Aikens, R. English, and C. Wolfe, "Power spectral density specifications for high-power laser systems," proceedings of *Specifications, Production, and Testing of Optical Components and Systems,* May 13-16, 1996, Glascow, Scotland, SPIE Proceedings Vol. 2775, 345-356 (1996).

2. W. Williams, "Numerical simulations of a phase corrector plate for NIF," presented to the *Third Annual International Conference on Solid State Lasers for Application to Inertial Confinement Fusion*, June 7-12, 1998, Monterey, California.